Solid Freeform Fabrication 2018: Proceedings of the 29th Annual International Solid Freeform Fabrication Symposium – An Additive Manufacturing Conference
Reviewed Paper

AN AEROSPACE INTEGRATED COMPONENT APPLICATION BASED ON SELECTIVE LASER MELTING: DESIGN, FABRICATION AND FE SIMULATION

Fei Liu[a], Wang Jingchao[b] ,Tan Zhi[b] ,Liu Bin[b] ,Guo Yue[b], David Z. Zhang[a,*]

[a] State Key Laboratory of Mechanical Transmission, Chongqing University, Chongqing 400044, China

[b] Beijing Institute of Aerospace Systems Engineering, Beijing 100076, China

Abstract: Developments in Additive Manufacturing (AM) technologies have enabled the integrated manufacturing of complex structures with multifunctional performances. Selective Laser Melting (SLM), as one of them, becomes the candidate for production of metallic aviation spaceflight structures because of its high precision for controlling architecture and excellent performance. An aerospace component named Upper-stage Cabin was selected for integrated design without connectors, and then manufactured by a SLM system using Ti-6Al-4V powder. The dimensional accuracy of the component was verified through testing; It's mechanical response was analyzed under compressive loading test, compared with the results of numerical simulation. The study found that SLM technology is an effective means for integrated design and manufacture of Upper-stage Cabin structures for aerospace. The dimensional precision of the complex integrated structures formed by SLM meets the application requirements. The formed integrated components have achieved good mechanical properties, which promote the application of this technology in aerospace field.

Keywords: additive manufacturing, selective laser melting, upper-stage cabin structure, integrated design and manufacturing

1. Introduction

Aerospace components featuring multifunctional performances including complex geometries, lightweight, high-performance and small production runs are difficult, costly, and time-consuming to manufacture. Additive Manufacturing (AM), a layer-by-layer process of joining materials to make objects from 3D model data, is becoming an appropriate solution for these challenges[1,2]. Compared with the conventional subtractive manufacturing methodologies, AM provides unprecedented opportunities for producing complex structures due to its freedom of manufacturing constraints, resulting in simplifying the design and reducing assembly or connection of aerospace components[3]. It meets the requirements of aerospace components with topological complexity resulting from integrated functions.

Selective laser melting (SLM), as one of AM technologies for metal forming, has developed rapidly in recent years[4]. Due to its excellent controllability of internal complex structures and good manufacturing accuracy, SLM shows a great capability to topologically

optimize component design with functional integration[5]. It has achieved direct integration in the aerospace field with the application of complex structural components[6]. A substantial weight and cycle reduction can be expected by using SLM for the integrated forming of multifunctional structure[7]. For example, one of the most compelling applications from GE Aviation is the new fuel nozzle fabricated using SLM, achieving the number reduction of parts from 18 to 1, and 25% weight reduction compared to previous component[8].

A wide range of materials including titanium and its alloys, nickel-based alloys, stainless and tool steels and some aluminum alloys are available for SLM technology[9]. With the increasing size of parts that can be fabricated by SLM equipment and the continuous expansion of the range of available materials, SLM is showing unique advantages in forming aerospace parts with large-scale and thin-walled complex structures.

In space application, the Upper-stage Cabin structure of space vehicle needs to withstand complex load environment, and provide installation and support platforms for the core system's instruments, an example one with complex structures and multifunctional performances is shown in Fig. 1. Therefore it usually exhibits a complex internal structure, at the same time, it is also required to provide good overall stiffness and strength. In addition, there are nearly a hundred machining and sheet metal forming parts installed inside the cabin structure, the manufacturing and assembling of them consume more than 50% of the total cabin cost, as well as the total cycle time. Integrated design and manufacturing are imperative in order to improve performance, reduce weight, and shorten the manufacturing cycle for aerospace components.

Fig. 1 An Upper-stage Cabin in aerospace application

In this work, a typical Upper-stage Cabin was selected for integrated design without connectors. In order to study the applicability of SLM technology in aerospace complex structures, a SLM equipment was used to realize the integrated manufacture of scaled Upper-stage Cabin. The dimensional accuracy of the as-build part was verified through testing; Upper-stage Cabin’s mechanical response was analyzed under compressive loading test, compared with the results of numerical simulation.

2. Experimental procedures

2.1 Materials and fabrication

The raw material in this work is gas-atomized prealloyed Ti-6Al-4V powders characterized by excellent mechanical properties and high strength-to-weight ratio. The Ti-6Al-4V powder have a chemical composition corresponding to ISO 5832-3, as listed in Table 1. Scanning electron microscope (SEM) images of the powders are presented in Fig. 2a and b with different magnifications. These powders are mostly spherical shapes with smooth surfaces, leading to a good flowability and a higher apparent density for SLM process. And they have a narrow particle size distribution with an average size of 33 μm.

Table 1 Chemical composition of Ti-6Al-4V (wt.%) provided by Electro Optical System (EOS) GmbH, Germany

Ti-6Al-4V	Ti	Al	V	O	N	C	H	Fe
Wt.%	(balance)	5.5—6.75	3.5—4.5	< 0.2	< 0.05	< 0.08	< 0.015	< 3

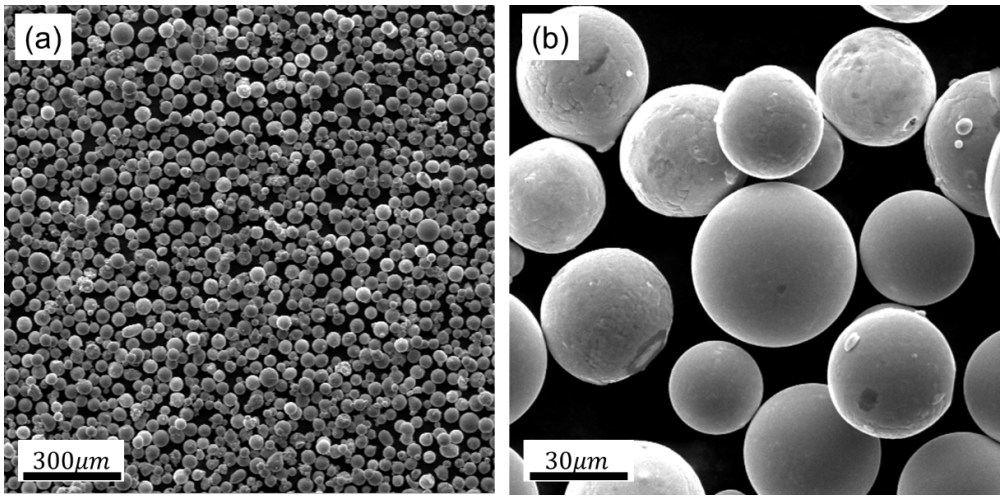

Fig. 2 SEM micrographs of the Ti-6Al-4V powder, ×100(a) and ×1000(b)

The aerospace component was manufactured by a SLM machine (EOSINT-M280, EOS GmbH, Germany) equipped with a 200 W CW Ytterbium fibre laser. The processing was performed at an argon protective atmosphere with O_2 content less than $0.1 vol.\%$ in the building chamber. And the processing parameters that have been optimized for the Ti-6Al-4V powder were set up as shown in Table 2. Under these conditions, the density of bulk Ti-6Al-4V was measured as $4.42\ g/cm^3 (\geq 99.5\%)$ by the Archimedes method. The mechanical properties of as-build tensile test piece are shown in Table 3.

Table 2 Processing parameters for Ti-6Al-4V

Parameters	Value
Laser power, W	175
Laser spot size, μm	100
Layer thickness, μm	30
Scanning speed, mm/s	125
Hatching space, mm	0.1

2.2 Test details

Uniaxial compression tests of the Upper-stage Cabin were conducted by using a universal testing machine equipped with a 200*KN* load cell(RMDW-200 from Ji'nan Rui Machinery Equipment Co., Ltd). The test applies axial pressure on the cabin through a thick steel plate loading tool, as shown in Fig. 6a. The compressive tests were carried out at a loading speed of 500*N/s*, accompanied by electronic strain gauges recording the local deformation behaviors of the Cabin.

In order to investigate suitability of the simulation method for the production based on the SLM process, the 3D FE analysis with the full sized model were performed for quasi-static simulations using ANSYS FE software. The CAD model of Upper-stage Cabin was imported into ANSYS where the beam element was used to simulate ribs with horizontal and vertical meshes, and the shell element was used to simulate the rest of the skins and the cross-beam structure. Material performance parameters used to this simulation are shown in the Table 3, which were measured by tensile test according to the ISO6892-1:2009 standard. The simulation test was performed according to the experimental conditions, and its results were compared with the experimental data.

Table 3 Material performance parameters of Ti-6Al-4V

Properties	Value
Elastic modulus, GPa	110
Poisson's ratio	0.34
Density, g/cm^3	4.43
Yield strength, MPa	1060
Tensile strength, MPa	1230

3. Results and discussion

3.1 Accuracy of Upper-stage Cabin fabricated by SLM

The main load-bearing structure of the cabin was extracted independently, establishing an integrated model with multiple components connected. Specifically, the integrated model is

mainly composed of cross-beam structure and grid-stiffened shells with two ellipse windows, as shown in Fig. 3. The cross-beam structure which has been studied in previous literature[10] was applied to realize lightweight design with thin-walled structures. And in order to meet the support-free requirement, chamfering optimization was performed for the horizontal ribs. Due to the size limitations of parts that can be formed in the existing SLM equipment, the model was scaled by 1:12 compared to the actual product, resulting in an overall cabin height ***(H_R)*** of 120*mm*, an outer diameter ***(D)*** of Ø200*mm*, a skin thickness ***(δ)*** of 0.5*mm*, shell grid's rib height ***(H_R)*** of 4*mm*, and rib width ***(a_R)*** of 1*mm*.

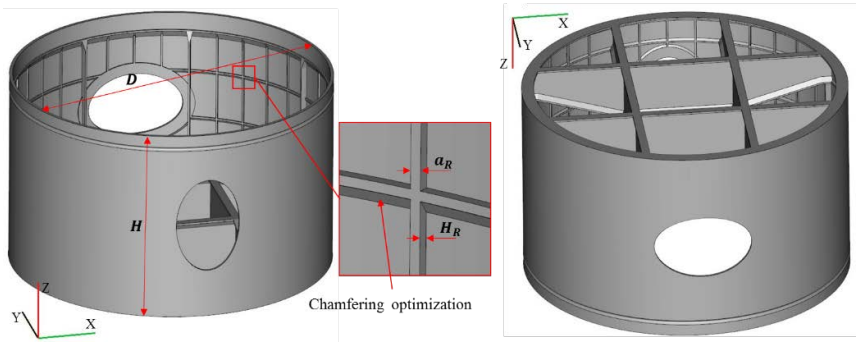

Fig. 3 A Upper-stage Cabin structure for aerospace application

The finished product is subjected to full-scale geometry measurements. Specifically, the thickness (***δ***) and the rib height (***H_R***) of the shell were measured using deep arch micrometer. The vertical rib width (***a_R***) of the grid, the outer diameter (***D***) and the height (***H***) of the shell are measured using a vernier caliper. Each measurement item was carried out at least 5 times to obtain the average values which are shown in Table 4.

Table 4 Comparison of main dimensions of Upper-stage Cabin

Measurement item	Designed size (mm)	Measurement size (mean: mm)	Error (%)
Thickness, ***δ***	0.50	0.65	30
Rib height, ***H_R***	4.00	3.99	-0.25
Vertical rib width, ***a_R***	1.00	1.19	19
Outer diameter, ***D***	200.00	199.90	-0.5
Height, ***H***	120.00	120.94	0.78

As can be seen from the above table, the studied Upper-stage Cabin produced by the SLM process has a relatively high precision meeting the requirements of aerospace components, indicating the capability of SLM suitble for manufacture of integrated structures with thin-walled features and complex structures.

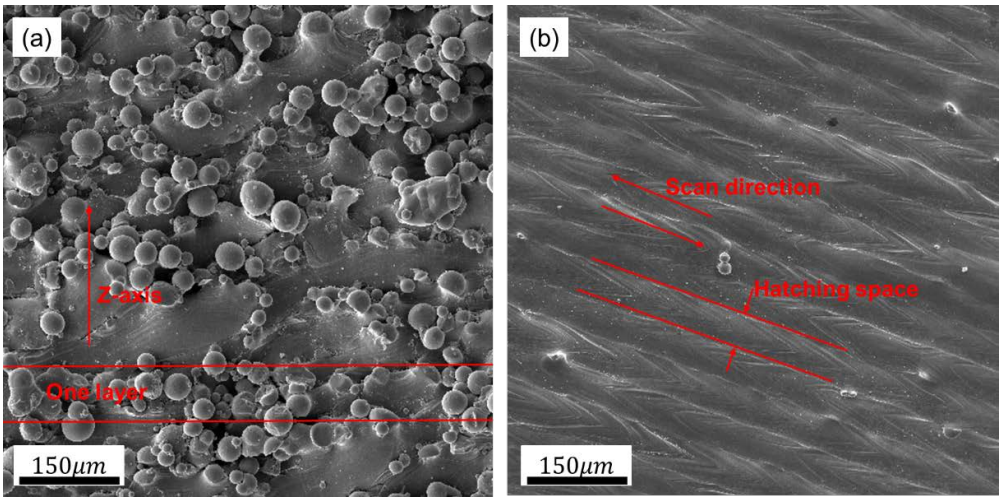

Fig. 4 SEM morphologies of the (a)side view and the (b) top view of Upper-stage Cabin

The SEM morphologies of the side view and the top view of Upper-stage Cabin are exhibited in Fig. 4. It is found there exist a lot of bonded particles on the side surface of Upper-stage Cabin, while there is almost none on the top surface. For SLM technology, the phenomenon of bonded particles is very common and unavoidable. The main reason for this phenomenon is that part of the powders at the contour boundary are partially melted and adhere to the surface[11]. On the top side of the part, all powders are melted as the laser spot moves, leaving a lot of noticeable scanning traces as shown in Fig. 4b. In our previous work[12], it has been found the roughness of side surface is Ra=40.04μm and top side Ra=17.18μm. The dimensional accuracy errors showed in table 3 come from these bonded particles, scanning traces and layer thickness as well[11].

3.2 Experimental and numerical simulation results

As shown in Fig. 5, there were 52 electronic strain gauges arranged on the Upper-stage Cabin, recording the local deformation behaviors of ribs and shell in different positions of cabin.

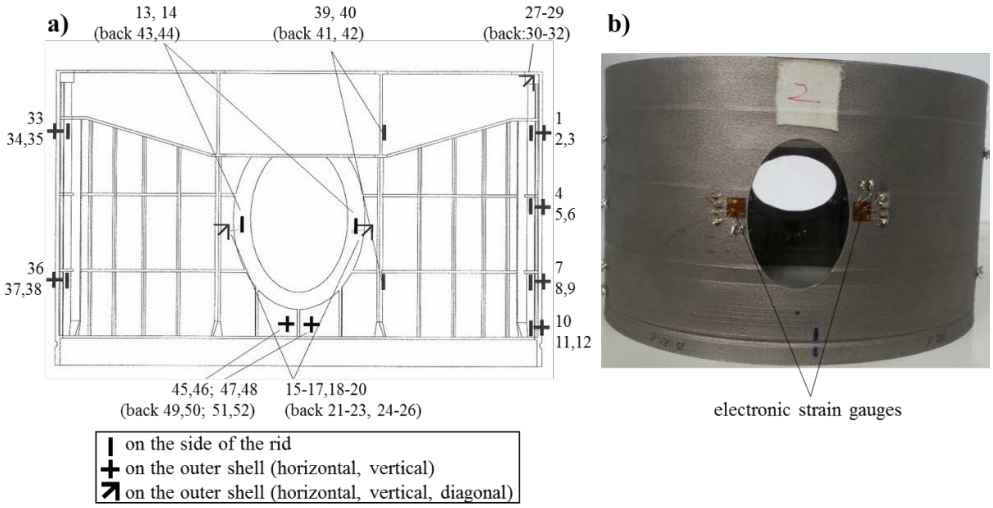

Fig. 5 a) Arrangement of electronic strain gauges,
b) as-build model with electronic strain gauges on one side

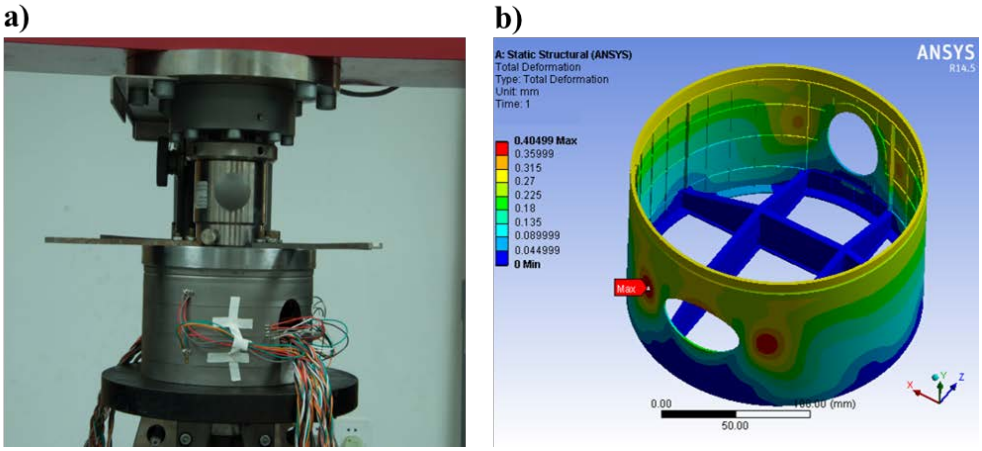

Fig. 6 a) Compressive experimental test monitored by electronic strain gauges;
b) Simulated strain images under 100*KN* loading

Fig. 6a shows the compressive experimental test monitored by electronic strain gauges. In this process, the load was gradually increased from 10*KN* to 100*KN*, and the data was extracted every 10*KN*. On the other hand, the numerical simulation method calculated the strain and displacement of the model under various loads. Fig. 6b exhibits the simulated strain images under 100*KN* loading. As expected, the largest total deformation occurs on both sides of the ellipse window, which were recording by electronic strain gauges multi-directionally.

Fig. 7 shows comparison between experimental and numerical results of total deformation at the first loading. It can be seen from the figure that the experimental results and the simulation results are in good agreement overall at both load of 10*KN* and 100*KN*, indicating the deformation behavior SLM manufacturing under the quasi-static conditions can be predicted through numerical simulation methods. Subsequently, Upper-stage Cabin was

subjected to the secondary loading under the stage of elastic deformation. The loading condition is the same as that of the first-time loading. The same results as the first loading are shown in Fig. 8, indicating the feasibility of the simulation method. In addition, like the theoretical design model, the integrated component of SLM manufacturing exhibits good performance consistency at different locations in the structure. This is mainly due to the fact that layer-by-layer processing of additive manufacturing weakens or even eliminates the adverse effect of structural complexity on performance. However, there were some points where the difference between experimental and numerical results is relatively large in both two loadings. It was found that most of these points were subjected to large deformations under experimental load, which have gone beyond the scope of linear analysis, so quasi-static linearity no longer applies to this stage.

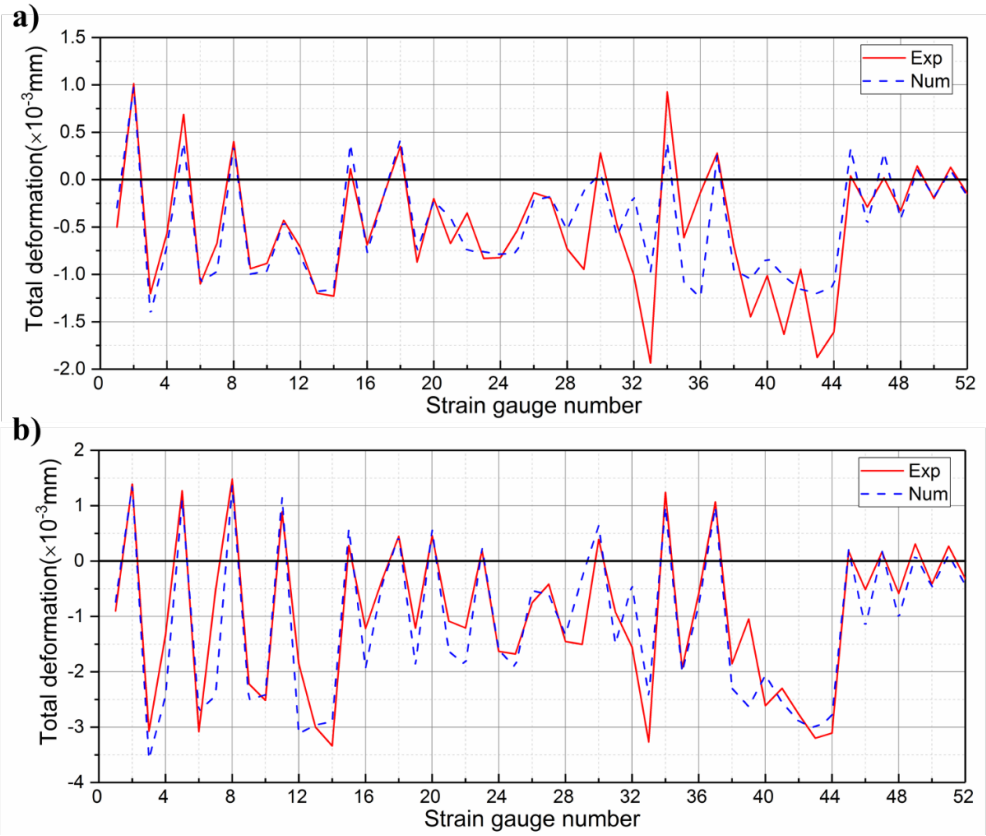

Fig. 7 The comparison between experimental and numerical results of total deformation at the first loading: a) load=10*KN*; b) load=100*KN*

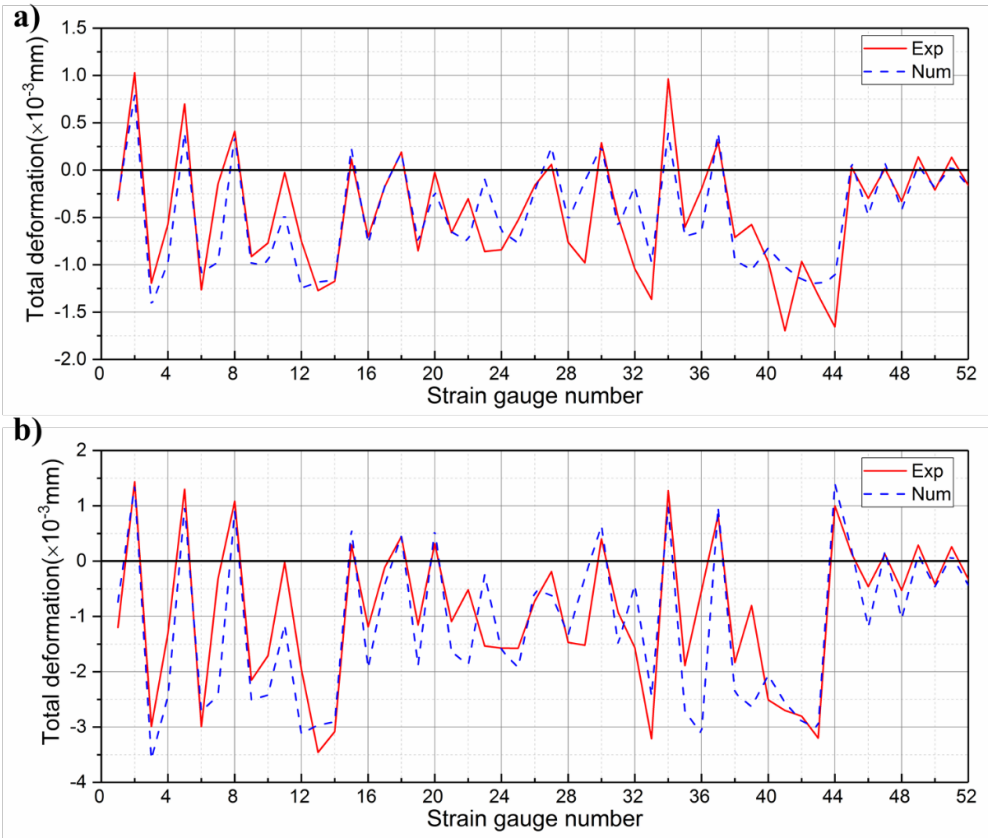

Fig. 8 The comparison between experimental and numerical results of total deformation at the second loading: a) load=10*KN*; b) load=100*KN*

3.3 Microstrutural analysis

There are many reasons for the error between the experimental results and the finite element simulation results, in which the difference of microstructure inside the parts may be the most critical factor. In the finite element analysis of the Upper-stage Cabin of this article, the analysis conditions are defined according to the traditional numerical simulation method. In fact, the internal microstructures of parts produced by the SLM are different from the ones produced by the traditional forming method.

Fig. 8a and b show the metallographic organization of the traditional rolling part and the as-build SLM manufacturing part, respectively. Fig. 9a,b show the metallographic organization of the traditional rolling part with different magnification. And Fig. 9c,d show the metallographic organization of SLM manufacturing part from the Upper-stage Cabin after test. From figures, it can be seen that metallographic structures of rolling state part exhibit a relatively large lamellar net arrangement characteristic, a typical $\alpha + \beta$ two-phase structure. The β-phase flakes are distributed around the coarse α-phase layer. The width of the α-phase is about $2\mu m$. While metallographic structure with elongated grains are shown in Fig. 8c and d for as-build SLM manufacturing part. This is due to the high temperature gradients that occur during the SLM process. The alloy forms fine microstructures in the rapid solidification process,

followed by the martensitic transformation, resulting in a fine acicular α′ structure.

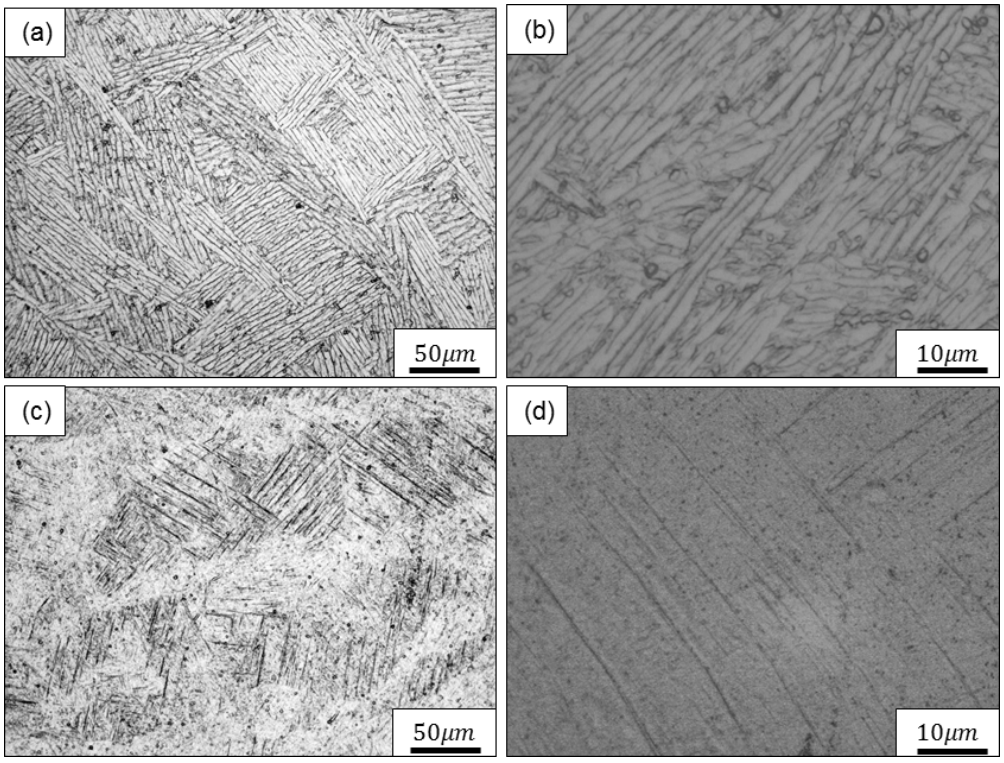

Fig. 9 Optical microstructure of rolling state(a, b), and as build of SLM(c, d)

4. Conclusion

In this study, an integrated component of aerospace Upper-stage Cabin was designed and then manufactured by SLM at a scale of 1:12 using Ti-6Al-4V alloy for aerospace applications. The feasibility of SLM technology for launch vehicle with complex integrated structures was verified in terms of manufacturing precision and mechanical properties. The experimental and numerical analysis were performed for testing the deformation behaviors under compressive load. It was found that the dimensional accuracy, mechanical properties, and simulation test results are in accordance with engineering practice, providing a basis for the more extensive application of SLM technology in aerospace structural products. In the future research, with a larger-sized SLM equipment, it will be possible to achieve a real integrated component at a scale of 1:1 designed and formed for aerospace application.

The study found that SLM technology is an effective means for integrated design and manufacture of Upper-stage Cabin structures for aerospace, which can significantly shorten the manufacturing cycle and reduce manufacturing processes, thereby reducing manufacturing costs.

Although new opportunities and benefits were provided by SLM technologies for manufacturing of aerospace integrated components, there are still some dynamic properties,

such as fatigue life, that need to be further studied. And with the development of SLM manufacturing in the future work, more accurate and larger size parts to be fabricated will be desirable for aerospace application.

Acknowledgments: The authors acknowledge the National High Technology Research and Development Program of China (863 Program: 2015AA042501) for financial support of this work.

Conflicts of Interest: The authors declare no conflict of interest.

References

1. Liu, R.; Wang, Z.; Sparks, T.; Liou, F.; Newkirk, J. *Aerospace applications of laser additive manufacturing*. 2017; p 351-371.
2. Allevi, G.; Cibeca, M.; Fioretti, R.; Marsili, R.; Montanini, R.; Rossi, G. Qualification of additively manufactured aerospace brackets: A comparison between thermoelastic stress analysis and theoretical results. *Measurement* **2018**, *126*, 252-258.
3. Wang, X.; Xu, S.; Zhou, S.; Xu, W.; Leary, M.; Choong, P.; Qian, M.; Brandt, M.; Xie, Y.M. Topological design and additive manufacturing of porous metals for bone scaffolds and orthopaedic implants: A review. *Biomaterials* **2016**, *83*, 127-141.
4. Thijs, L.; Verhaeghe, F.; Craeghs, T.; Humbeeck, J.V.; Kruth, J.-P. A study of the micro structural evolution during selective laser melting of ti-6al-4v. *Acta. Mater.* **2010**, *58*, 3303-3312.
5. Xu, W.; Brandt, M.; Sun, S.; Elambasseril, J.; Liu, Q.; Latham, K.; Xia, K.; Qian, M. Additive manufacturing of strong and ductile ti–6al–4v by selective laser melting via in situ martensite decomposition. *Acta. Mater.* **2015**, *85*, 74-84.
6. Seabraa, M.; Azevedob, J.; Araújoa, A.; Reis, L. Selective laser melting (slm) and topology optimization for lighter aerospace componentes. *Procedia Structural Integrity* **2016**.
7. Bici, M.; Brischetto, S.; Campana, F.; Ferro, C.G.; Seclì, C.; Varetti, S.; Maggiore, P.; Mazza, A. Development of a multifunctional panel for aerospace use through slm additive manufacturing. *Procedia CIRP* **2018**, *67*, 215-220.
8. Kellner, T. Fit to print: New plant will assemble world's first passenger jet engine with 3d printed fuel nozzles, next-gen materials. 2014.
9. Yap, C.Y.; Chua, C.K.; Dong, Z.L.; Liu, Z.H.; Zhang, D.Q.; Loh, L.E.; Sing, S.L. Review of selective laser melting: Materials and applications. *Applied Physics Reviews* **2015**, *2*, 041101.
10. Li, Z.; Zhang, D.Z.; Dong, P.; Kucukkoc, I. A lightweight and support-free design method for selective laser melting. *The International Journal of Advanced*

Manufacturing Technology **2016**, *90*, 2943-2953.

11. Yan, C.; Hao, L.; Hussein, A.; Raymont, D. Evaluations of cellular lattice structures manufactured using selective laser melting. *International Journal of Machine Tools and Manufacture* **2012**, *62*, 32-38.
12. Li, Z.; Kucukkoc, I.; Zhang, D.Z.; Liu, F. Optimising the process parameters of selective laser melting for the fabrication of ti6al4v alloy. *Rapid Prototyping J.* **2018**, *24*, 150-159.